ACCELERATED COMMUNICATION

Atomic structure of the cross-β spine of islet amyloid polypeptide (amylin)

JED J.W. WILTZIUS,[1] STUART A. SIEVERS,[1] MICHAEL R. SAWAYA,[1] DUILIO CASCIO,[1] DMITRIY POPOV,[2] CHRISTIAN RIEKEL,[2] AND DAVID EISENBERG[1]

[1]Howard Hughes Medical Institute, UCLA-DOE Institute for Genomics and Proteomics, Los Angeles, California 90095-1570, USA
[2]European Synchrotron Radiation Facility, BP 220, F-38043 Grenoble Cedex, France

(RECEIVED May 18, 2008; FINAL REVISION June 9, 2008; ACCEPTED June 10, 2008)

Abstract

Human islet amyloid polypeptide (IAPP or amylin) is a 37-residue hormone found as fibrillar deposits in pancreatic extracts of nearly all type II diabetics. Although the cellular toxicity of IAPP has been established, the structure of the fibrillar form found in these deposits is unknown. Here we have crystallized two segments from IAPP, which themselves form amyloid-like fibrils. The atomic structures of these two segments, NNFGAIL and SSTNVG, were determined, and form the basis of a model for the most commonly observed, full-length IAPP polymorph.

Keywords: IAPP; amylin; amyloid; aggregation; type 2 diabetes; protein crystallization

Supplemental material: see www.proteinscience.org

Islet amyloid polypeptide (IAPP, also called amylin) is associated with type II diabetes, a disease that has increased over the past two decades and now afflicts an estimated 20 million people in America and 100 million worldwide (Hossain et al. 2007). No consensus exists regarding the etiology of the disease, although the initial phase appears to be characterized by a condition of insulin resistance (Saltiel 2001). Pancreatic extracts from individuals with type II diabetes have been found to contain extracellular deposits of the 37-residue peptide hormone IAPP that is expressed, stored, and secreted from the β-islet cells of the pancreas (Cooper et al. 1987; Westermark et al. 1987; Cooper 1994). IAPP was first identified in 1987, and is considered a potential target for the treatment of diabetes (Schmitz et al. 2004; Yan et al. 2006).

Reprint request to: David Eisenberg, Howard Hughes Medical Institute, UCLA-DOE Institute for Genomics and Proteomics, Los Angeles, CA 90095-1570, USA; e-mail: david@mbi.ucla.edu; fax: (310) 206-3914.

Article and publication are at http://www.proteinscience.org/cgi/doi/10.1110/ps.036509.108.

The role of IAPP in diabetes is uncertain (Höppener et al. 2002), but there is mounting evidence for the importance of amyloid formation associated with this disease. Ninety-five percent of diagnosed individuals stain positive postmortem for pancreatic amyloid deposits composed of mature, fibrillar IAPP (Höppener et al. 2000). The extent of amyloid deposition correlates with disease severity (Esapa et al. 2005). Both synthetic and endogenous IAPP have been shown to display significant cytotoxicity to cultured islet cells (de Koning et al. 1994; Kapurniotu 2001; Konarkowska et al. 2006). This cytotoxicity is believed to be related to islet cell death that occurs in diabetes, leading to loss of blood glucose homeostasis and subsequent insulin dependence (Ritzel et al. 2007). Mouse IAPP does not form amyloid, and differs from human in only six of 37 residues (Nishi et al. 1989). Supporting the relationship of fibrillation of IAPP to type II diabetes is the observation that mice do not develop type II diabetes, yet transgenic mice expressing human IAPP can develop the disease (Fox et al. 1993).

The fibrillar form of IAPP has been studied intensively, and amyloidogenic regions within IAPP have been

identified. Using coordinated X-ray fiber diffraction, electron diffraction, and cryo-EM, Sumner Makin and Serpell (2004) examined the ultrastructure of fibrils of IAPP, concluding that the fibrils are made up of extended strands running perpendicular to the fibril axis, 4.7 Å apart, as is found in the ''cross-β'' structure of other amyloid-like fibrils (Eanes and Glenner 1968). Langen and coworkers (Jayasinghe and Langen 2004) determined these β-strands to be in a parallel orientation using electron paramagnetic resonance spectroscopy. Recent studies have reported a structural motif common to short microcrystalline segments derived from a variety of amyloid-forming proteins. It consists of two β-sheets with interdigitated side chains, and is called a steric zipper (Nelson et al. 2005; Sawaya et al. 2007).

Several peptide segments derived from the amino acid sequence of IAPP are capable of forming amyloid-like fibrils, with previous work suggesting that the segment containing residues 22–29 (NFGAILSS) forms the spine of the fibril under physiological conditions (Westermark et al. 1990; Moriarty and Raleigh 1999; Goldsbury et al. 2000; Tenidis et al. 2000). Various polymorphic forms of IAPP fibrils were described by Goldsbury et al. (1997), and modeled by Kajava et al. (2005), and a full atomic model of a single polymorph has been proposed by Luca et al. (2007) based on constraints from solid-state NMR.

Attempts to crystallize full-length IAPP in either a native or fibrillar form have been unsuccessful. Here we report the crystallization of two segments from IAPP spanning the putative amyloidogenic domain. The structures of these segments, NNFGAIL and SSTNVG, were determined. These segments constitute residues 21–27 and 28–33 from IAPP, respectively. The structures of these segments in the amyloid-like state were used in combination with biochemical and structural data from others to formulate an atomic-based structural model of an amyloid fibril.

Results and Discussion

Fibril-forming segments of IAPP

To confirm and extend earlier work indicating that the segment of IAPP between residues 23 and 37 is crucial to fibril formation, we used several methods. We began with the 3D profile method to computationally predict segments from IAPP that have high fibril-forming potential (Thompson et al. 2006). The hexameric segments NNFGAI and SSTNVG, spanning residues 21 to 33, are located toward the C terminus of the 37-residue IAPP and score highly with this method (data not shown). The computational predictions that these segments drive fibrillation are reinforced by our experimental finding that while a maltose binding protein (MBP)-IAPP fusion protein forms fibrils under physiological conditions, the MBP–IAPP 1–22 fusion does not (Fig. 1A,B). MALDI-TOF mass spectrometry analysis of purified fibrils confirmed that they contain the full-length MBP–IAPP construct (data not shown).

As a further guide to understand how IAPP forms fibrils, we compared fibril-forming human IAPP to mouse IAPP, which does not fibrillize (Westermark et al. 1990). As shown in Figure 1C, mouse IAPP differs from human IAPP in only six residues, five of which are in the segment 23–29 implicated above in fibril formation. The following fibrillation experiments were performed on an IAPP 8–37 construct, omitting the first seven residues which do not affect the de novo kinetics of fibril formation (Koo and Miranker 2005). Note that these experiments were performed with 1% hexafluoroisopropanol (HFIP). HFIP and other helical promoting agents are known to accelerate the kinetics of IAPP fibril formation (Larson and Miranker 2004; Jayasinghe and Langen 2007). The residue replacements shown in Figure 1D demonstrate that residue 18, the most N-terminal of these six positions, does not affect de novo fibrillation. Insulin is a competitive inhibitor of IAPP fibrillation (Larson and Miranker 2004), and Figure 1E shows that the H18R substitution slightly reduces this insulin-induced inhibition. The conservative F23L substitution increases the lag to fibrillation, supporting a role for phenylalanine in the nucleation of fibril formation (Gazit 2002; Tracz et al. 2004). The H18R/F23L replacements display an even greater lag time, suggesting cooperativity between residues 18 and 23 during fibrillation. The H18R/S28P/S29P substitutions failed to form fibrils in the time frame of our experiment, suggesting that although the human residues within the 22–27 (NFGAIL) segment are required for fibril formation, the proline substitutions can prevent conversion. The H18R/F23L/A25P/I26P substitutions also failed to form fibrils, showing that a construct containing human residues 28–33 (SSTNVG), but not the human residues in the 22–27 segment, also fails to maintain normal human 8–37 fibril formation kinetics. In short, both the 3D profile method and the data of Figure 1 confirm that segment 22–29 (NFGAILSS) is important for fibril formation.

Atomic structures of the amyloid-like segments NNFGAIL and SSTNVG

The atomic structure of IAPP in its fibrillar form is not known. Our attempts to crystallize full-length IAPP in the fibrillar state have been unsuccessful, so we approached this problem by crystallizing hepta- and hexapeptide segments from the C-terminal, fibril-forming portion of IAPP. We selected these segments based both on our 3D profile method and the fibril-forming assays described

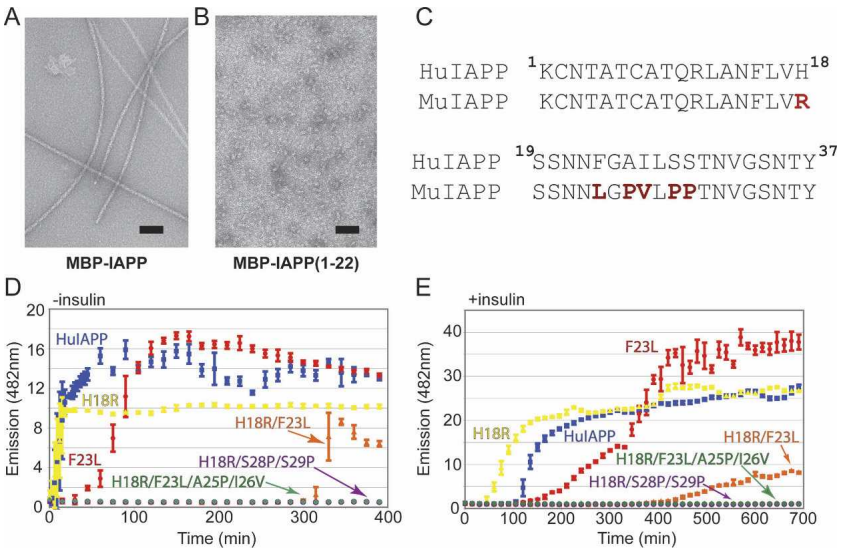

Figure 1. IAPP residues 23–37 are necessary for fibril formation of IAPP. (*A*) The MBP–IAPP construct forms amyloid fibrils as visualized by electron microscopy. The scale bar represents 100 nm. These fibrils were determined to contain the full-length construct by mass spectrometry. (*B*) The MBP–IAPP 1–22 construct failed to form fibrils. (*C*) The fibril-forming sequence of human IAPP is compared to that of the nonfibril-forming mouse IAPP, with residue differences noted in red. (*D*) The effects of residue replacements on the rate of fibrillation of IAPP. Histidine 18 of human IAPP is the only residue difference between human and mouse IAPP in the N-terminal region. This residue difference appears to have no effect on the fibril formation of IAPP, whereas the subtle F23L replacement delays fibrillation. The double mutant (H18R/F23L) shows an even greater lag time, suggesting cooperativity between these sites during fibril formation. The H18R/S28P/S29P triple mutant shows that although IAPP 22–27 may be required for fibril formation, the downstream proline substitutions can prevent conversion to amyloid fibrils. (*E*) Insulin increases the lag time prior to fibrillation. This affect appears to be slightly less potent with the H18R substitution.

above. Both NNFGAIL and SSTNVG segments formed amyloid-like fibrils as well as microcrystals, and we determined their atomic structures as shown in Figure 2.

The crystal structure of SSTNVG resembles that of other fibril-forming segments from fibril-forming proteins (Nelson et al. 2005; Sawaya et al. 2007). Each SSTNVG segment forms hydrogen bonds with identical segments 4.8 Å above and below it, in an extended parallel β-sheet. Two such sheets face each other with their protruding side chains interdigitating (Fig. 2D), and extend the whole length of the fibril-like structure in the needle-shaped crystals. The interface between the two sheets is devoid of water; thus SSTNVG forms a Class I steric zipper (Sawaya et al. 2007), characteristic of several segments of other protein segments associated with amyloid and prion diseases. The substantial shape complementarity (Sc = 0.85) and area buried (234 Å^2) are also characteristic of other steric zippers (Lawrence and Colman 1993; Sawaya et al. 2007). An unusual feature of this structure is that the side chains of Ser29 residues extend across the interface to form a hydrogen bond with one another, the ''kissing serines'' seen in Figure 2D.

The structure of the NNFGAIL segment is not a typical steric zipper. It contains a pronounced bend in the backbone facilitated by a Gly in the fourth position. This bend allows the side chain of Asn in the second position to turn inward and to hydrogen bond to the backbone carbonyl of the Gly residue. The structure also lacks the interdigitated side chains of the steric zipper motif. This peptide instead has a tight main chain–main chain interface formed by Phe, Gly, and Ala residues from opposing sheets separated by ~3 Å (Fig. 2C). This interface has a shape complementarity of 0.90 and an area buried of 230 Å^2. The main-chain carbonyl of the Phe is tilted within the backbone and is hydrogen bonding with a neighboring main-chain amide across this dry interface. The Phe side chain adopts a rotamer that favors this main-chain packing. In short, the NNFGAIL segment may form a turn leading into a steric zipper, formed from two sheets made up of SSTNVG segments. This model for full-length IAPP is discussed below.

IAPP fibrillar structure

IAPP forms numerous distinct fibril morphologies, with each polymorph believed to be a consequence of a unique atomic packing of the spine (Goldsbury et al. 1997; Tycko 2004; Kodali and Wetzel 2007). Consistent with this view, we have discovered several overlapping segments of IAPP that each form fibrils and needle-shaped microcrystals typical of steric zipper structures (data not shown) (Sawaya et al. 2007). A steric zipper formed by

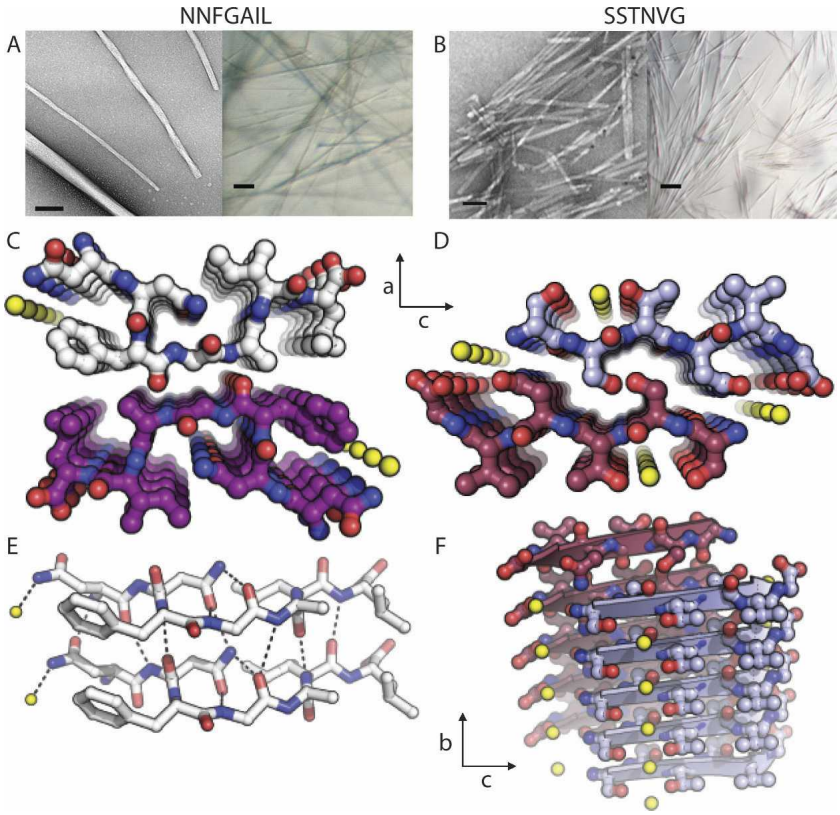

Figure 2. Structures of the NNFGAIL and SSTNVG amyloid-like segments of IAPP. The NNFGAIL (*A*) and SSTNVG (*B*) segments, which abut in IAPP, are capable of forming amyloid-like fibrils (*left* panels) and microcrystals (*right* panels), respectively. The scale bars are 100 nm for the electron microscopy images (*left* panels) and 50 μm for the light microscopy images (*right* panels). (*C*) The structure of NNFGAIL, consisting of two close-packed β-sheets, viewed *down* the sheets. Notice the pronounced bend in the backbone, but not the usual interpenetration of side chains found in the steric zipper. Instead, NNFGAIL displays a dry, main chain–main chain zipper-like interface. Water molecules are shown as yellow spheres, and are *outside* the intersheet interface in both NNFGAIL and SSTNVG. (*D*) The structure of SSTNVG, viewed *down* the β-sheets shows the interdigitated side chains between adjacent β-sheets across a dry, steric zipper interface. (*E*) Two layers of the NNFGAIL structure, shown as stick molecules, showing the hydrogen bonds between layers. (*F*) Five layers of the SSTNVG structure viewed from the wet interface. Notice that *E* and *F* are 90° from the views of *C* and *D*.

one of these segments within an IAPP molecule would preclude the formation of a steric zipper within another segment of the same molecule. For example, the R18H single-residue substitution in mouse IAPP renders this construct capable of forming fibrils (Green et al. 2003). This construct retains all five mouse residues in the putative amyloidogenic domain (Fig. 1C) including the three prolines at positions 25, 28, and 29. In this construct, we believe that one of the other segments is forming the zipper spine. Thus, the multiplicity of fibril-forming segments suggests a multiplicity of fibrillar polymorphs of IAPP, as has been observed by others.

In Figure 3 we present an atomic model for the most common IAPP fibril polymorph observed by Goldsbury et al. (1997). This fibril has a width of ~6.4 nm and crossover distance of 25 nm. Our model is based on our SSTNVG structure, and also incorporates the bent backbone of our structure for the NNFGAIL segment. Each IAPP molecule is in an extended β-conformation with a hairpin turn, and is stacked on the molecule below to form two β-sheets. In our model, SSTNVG segments contributed by pairs of IAPP molecules are interdigitated about a 2_1 axis, which runs along the axis of the fibril, bisecting the line between the second Ser residues of each SSTNVG segment (Fig. 3A). The facing SSTNVG segments create a steric zipper that extends into the four C-terminal residues of IAPP, which interact with the termination of the NNFGAIL turn of the opposing molecule. This places Phe 23 and Tyr 37 of opposing molecules well within the 10.2 Å threshold established by fluorescence resonance energy transfer (FRET) (Padrick and Miranker 2001). The side chains of the Phe and Tyr residues stack as predicted by Gazit (Azriel and Gazit 2001; Gazit 2002). Thus, the fibril contains four parallel

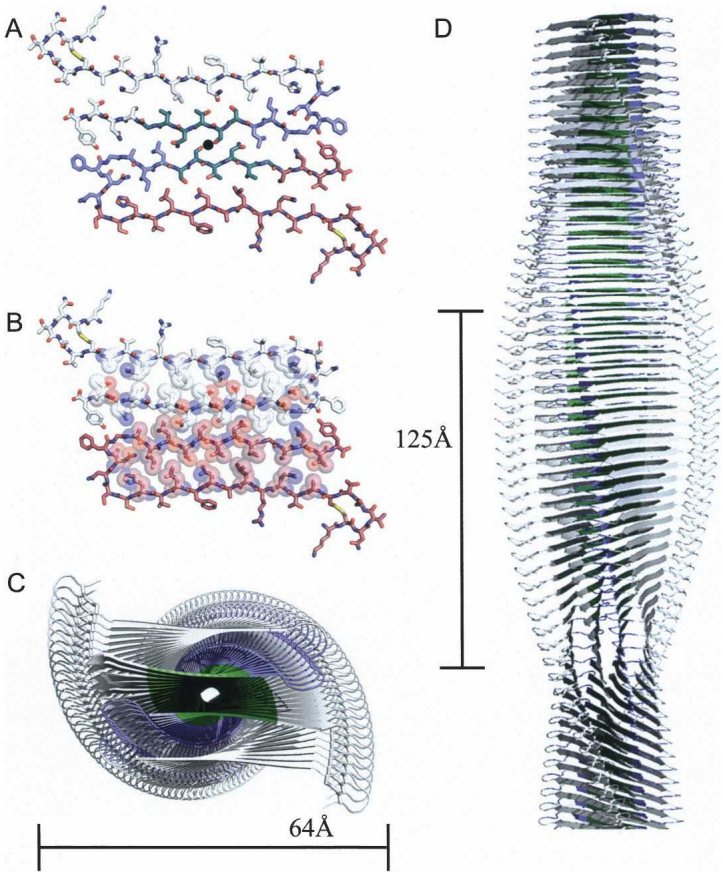

Figure 3. Model of an IAPP fibril based on our crystal structures of NNFGAIL and SSTNVG. (*A*) View *down* the fibril axis (shown by the black dot). Two molecules of IAPP mate in a dry steric zipper around the fibril axis. The segment NNFGAIL, shown in blue in each IAPP molecule, is part of the hairpin turn and the start of the long steric zipper interface. The extension of the central strand, and its mating strand, contain the SSTNVG zipper interface, shown in green in each IAPP molecule. The final four residues of IAPP are modeled to complete the zipper interface. The initial 20 residues of IAPP are modeled to complete the outer strands of the two sheets, and to form the cyclic disulfide bridge near the N terminus. (*B*) Space-filling representation shows the tight steric zipper interface between residues 23 and 37 on the two IAPP molecules. (*C*) View *down* the axis of the fibril with a diameter of 64 Å. The modeled residues are shown in white and the residues corresponding to our crystal structures are shown in blue for NNFGAIL and green for SSTNVG. (*D*) View *perpendicular* to the fibril axis of the same fibril with a length of 125 Å (one-quarter of a full turn), showing the 4.8 Å spacing that gives rise to the strong meridional reflection of the fibril diffraction pattern. This model has a mass per unit length and crossover distance that agrees closely with the experimental value for the most commonly observed polymorphic fibril.

β-sheets, the central two constituting the dry steric zipper (Fig. 3C).

We have chosen the SSTNVG segment as the centerpiece of the model because its intersheet distance in the crystal structure corresponds more closely with the observed equatorial reflections in the fiber diffraction pattern. This packing, observed in the SSTNVG crystal structure, can be extended throughout the 23–37 segment, which is consistent with the FRET data (Padrick and Miranker 2001). We did not choose NNFGAIL for the center of the fibril because the spacing in the crystal structure between NNFGAIL sheets is not in agreement with the fiber diffraction data, and the close main chain packing in NNFGAIL would not allow for extension of side chain packing beyond this segment.

We modeled the N terminus of IAPP (residues 8–17) as a short β-strand on the periphery of the fibril in the absence of other information about its structure. The model was optimized to reduce steric clashes and improve hydrogen-bonding geometry. The model has a diameter of 64 Å and incorporates a left-handed twist of 3.4° per layer, consistent with the observed crossover distance of 25 nm for a fibril of IAPP (Green et al. 2004). The simulated X-ray fiber diffraction pattern of our model is in reasonable agreement with the full-length experimental diffraction pattern of IAPP and in excellent agreement with the fiber diffraction pattern of fibrils composed of IAPP 23–37 (Fig. 4A,B; Supplemental Fig. S1; Sumner Makin and Serpell 2004). Moreover, the calculated mass per unit length of our fibril of 16.3 kDa/nm is in

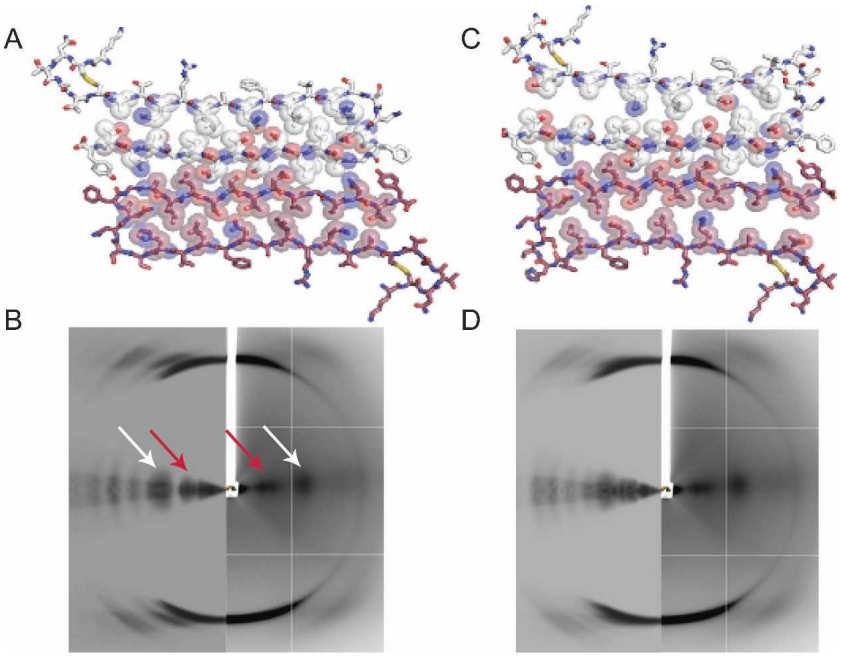

Figure 4. Comparison of the simulated fibril diffraction patterns of fibril models with the experimental diffraction images of IAPP 23–37. The 23–37 segment represents the steric zipper spine of the fibril and is the segment of highest confidence in the model. Space-filling representations are shown for our models (*A,C*). The simulated fiber diffraction patterns, obtained by Fourier-transforming these models, are shown on the *left* halves and the experimental diffraction pattern for the IAPP 23–37 segment are shown on the *right* halves of *B* and *D*. The hallmark 4.78 Å meridional reflection characteristic of the hydrogen bonding axis is observed. The arrows in *B* indicate equatorial reflections at ~15 Å (red) and ~8.5 Å (white) that match between the simulated model and experimental diffraction patterns.

reasonable agreement with the STEM measured values of Goldsbury et al. (1997) of 20 kDa/nm, and of Luca et al. (2007) of 13–19 kDa/nm.

Recently, two other atomic models have been proposed for IAPP fibrils. Both, like ours, stack IAPP molecules in β-conformation on top of one another, perpendicular to the fibril axis, to form extended β-sheets parallel to the fibril axis. Kajava et al.'s (2005) ''serpentine'' model is for a protofibril with the narrow cross section of 45–55 Å. It features one IAPP molecule per 4.7 Å layer, folded into three segments, thus producing three β-sheets that run the length of the fibril. Kajava et al. (2005) argue that this model is consistent with the mass-per-unit-length measurements for higher order fibrils. The serpentine model differs from ours also in that its three sheets do not closely interdigitate into one another, as found in the steric zippers of known structure.

A very recent model proposed by Tycko and coworkers was based on distance constraints from solid-state NMR (Luca et al. 2007). The Tycko model is similar to ours in proposing two IAPP molecules per 4.8 Å layer, also organized into four sheets. The principal difference is that the sheets of the Tycko model do not interdigitate as closely as the sheets in our model, based on the SSTNVG structure. The second main difference is in the registration of the two inner sheets. The Tycko model obeys a distance constraint of 6 Å between the side chains of either Asn14 or Tyr15 and Ile26 and Leu27, whereas in our model these two residues are spaced further apart (12 Å). After the recent publication of the Tycko model, we computed an alternative model (Fig. 4C), which is similar to the model of Figure 3 in adhering to our experimental SSTNVG and NNFGAIL structures, but which introduces the Tycko distance constraint. The central steric zipper of the alternative model remains the same, but the two strands within the same molecule no longer align as well as in our original model (as shown in the space-filling representations of Fig. 4A and C). In short, solid-state NMR and X-ray approaches have yielded similar models, which, however, differ in the details of the packing of side chains.

Materials and Methods

Fibril formation assays

All peptides (CSbio) were first solublized in 100% Hexafluoroisopropanol (HFIP) to a stock concentration of 1 mM. Reaction conditions were 20 mM sodium acetate pH 6.5 and 10 μM Thioflavin T. Peptides were diluted 1/100 into this mixture then

spin filtered to remove any potential preformed aggregates that may have been created during synthesis. The total reaction volume was 200 μL with final concentrations of 10 μM peptide and 1% HFIP. The addition of 150 mM sodium chloride did not have an effect on the kinetics of fibril formation (as determined by electron microscopy) but caused strong fluctuations in ThT fluorescence. A sample was taken from each reaction immediately after filtering to confirm the absence of any fibrils or preformed aggregates prior to the start of the assay. Samples were performed in triplicate and fluorescence measurements were taken every 3 min. The average of five time points is shown on the representative graph. The standard deviation of the time points is shown as error bars. Samples were taken at pertinent time points for analysis by electron microscopy to confirm the presence or absence of fibrils as seen by ThT binding.

Segment crystallization and structure determination

The NNFGAIL and SSTNVG segments were solublized in water to 2 mg/mL. Both peptides were spin filtered (0.22 micron) prior to crystallization. The NNFGAIL peptide was crystallized in 20% ethylene glycol, and the SSTNVG peptide was crystallized in 30% MPD. X-ray data for NNFGAIL were collected at ESRF microfocal beamline ID13. The SSTNVG data were collected at the SLS beamline X06SA. Statistics pertaining to structure determination are provided in the Supplemental data (Supplemental Table 1). The fiber diffraction images of IAPP 23–37 were taken at the APS beamline 24ID-C. The coordinates have been deposited in the Protein Data Bank with accession codes 3DG1 for SSTNVG and 3DGJ for NNFGAIL.

Fibril modeling

A fibril model was built around the SSTNVG fibril core. Using COOT and O (Jones et al. 1991; Emsley and Cowtan 2004), we linked the NNFGAIL segment structure with the SSTNVG structure and built in the rest of the molecule. Model building was guided by calculated fibril diffraction patterns (Sawaya et al. 2007). CNS was used to minimize the energy of the model by optimizing hydrogen bonding and removing steric clashes (Brunger et al. 1998). PyMOL, from DeLano Scientific, was used to create the figures.

Acknowledgments

We thank J. Bowie, G. Chanfreau, and T. Yeates for discussion, J. Whitelegge and A. Laganowsky for assistance with mass spectrometry, L. Goldschmidt for the 3D profile scan of IAPP, and NIH, NSF, and HHMI for support. We also thank Dr. A.V. Kajava and R. Tycko for releasing to us the atomic coordinates of the superpleated β-structure and solid-state NMR models for IAPP, respectively.

References

Azriel, R. and Gazit, E. 2001. Analysis of the minimal amyloid-forming fragment of the islet amyloid polypeptide. An experimental support for the key role of the phenylalanine residue in amyloid formation. *J. Biol. Chem.* **276:** 34156–34161.

Brunger, A.T., Adams, P.D., Clore, G.M., DeLano, W.L., Gros, P., Grosse-Kunstleve, R.W., Jiang, J.S., Kuszewski, J., Nilges, M., Pannu, N.S., et al. 1998. Crystallography & NMR system: A new software suite for macromolecular structure determination. *Acta Crystallogr. D Biol. Crystallogr.* **54:** 905–921.

Cooper, G.J. 1994. Amylin compared with calcitonin gene-related peptide: Structure, biology, and relevance to metabolic disease. *Endocr. Rev.* **15:** 163–201.

Cooper, G.J.S., Willis, A.C., Clark, A., Turner, R.C., Sim, R.B., and Reid, K.B.M. 1987. Purification and characterization of a peptide from amyloid-rich pancreases of type 2 diabetic patients. *Proc. Natl. Acad. Sci.* **84:** 8628–8632.

de Koning, E.J.P., Morris, E.R., Hofhuis, F.M.A., Posthuma, G., Höppener, J.W.M., Morris, J.F., Capel, P.J.A., Clark, A., and Verbeek, J.S. 1994. Intra- and extracellular amyloid fibrils are formed in cultured pancreatic islets of transgenic mice expressing human islet amyloid polypeptide. *Proc. Natl. Acad. Sci.* **91:** 8467–8471.

Eanes, E. and Glenner, G. 1968. X-ray diffraction studies on amyloid filaments. *J. Histochem. Cytochem.* **16:** 673–677.

Emsley, P. and Cowtan, K. 2004. Coot: Model-building tools for molecular graphics. *Acta Crystallogr. D Biol. Crystallogr.* **60:** 2126–2132.

Esapa, C., Moffitt, J.H., Novials, A., McNamara, C.M., Levy, J.C., Laakso, M., Gomis, R., and Clark, A. 2005. Islet amyloid polypeptide gene promoter polymorphisms are not associated with type 2 diabetes or with the severity of islet amyloidosis. *Biochim. Biophys. Acta* **1740:** 74–78.

Fox, N., Schrementi, J., Nishi, M., Ohagi, S., Chan, S.J., Heisserman, J.A., Westermark, G.T., Leckstrom, A., Westermark, P., and Steiner, D.F. 1993. Human islet amyloid polypeptide transgenic mice as a model of non-insulin-dependent diabetes mellitus (NIDDM). *FEBS Lett.* **323:** 40–44.

Gazit, E. 2002. A possible role for π-stacking in the self-assembly of amyloid fibrils. *FASEB J.* **16:** 77–83.

Goldsbury, C., Goldie, K., Pellaud, J., Seelig, J., Frey, P., Muller, S.A., Kistler, J., Cooper, G.J.S., and Aebi, U. 2000. Amyloid fibril formation from full-length and fragments of amylin. *J. Struct. Biol.* **130:** 352–362.

Goldsbury, C.S., Cooper, G.J.S., Goldie, K.N., Muller, S.A., Saafi, E.L., Gruijters, W.T.M., Misur, M.P., Engel, A., Aebi, U., and Kistler, J. 1997. Polymorphic fibrillar assembly of human amylin. *J. Struct. Biol.* **119:** 17–27.

Green, J., Goldsbury, C., Mini, T., Sunderji, S., Frey, P., Kistler, J., Cooper, G., and Aebi, U. 2003. Full-length rat amylin forms fibrils following substitution of single residues from human amylin. *J. Mol. Biol.* **326:** 1147–1156.

Green, J.D., Goldsbury, C., Kistler, J., Cooper, G.J.S., and Aebi, U. 2004. Human amylin oligomer growth and fibril elongation define two distinct phases in amyloid formation. *J. Biol. Chem.* **279:** 12206–12212.

Höppener, J.W.M., Ahren, B., and Lips, C.J.M. 2000. Islet amyloid and type 2 diabetes mellitus. *N. Engl. J. Med.* **343:** 411–419.

Höppener, J.W.M., Nieuwenhuis, M.G., Vroom, T.M., Ahren, B., and Lips, C.J.M. 2002. Role of islet amyloid in type 2 diabetes mellitus: Consequence or cause? *Mol. Cell. Endocrinol.* **197:** 205–212.

Hossain, P., Kawar, B., and El Nahas, M. 2007. Obesity and diabetes in the developing world—a growing challenge. *N. Engl. J. Med.* **356:** 213–215.

Jayasinghe, S.A. and Langen, R. 2004. Identifying structural features of fibrillar islet amyloid polypeptide using site-directed spin labeling. *J. Biol. Chem.* **279:** 48420–48425.

Jayasinghe, S.A. and Langen, R. 2007. Membrane interaction of islet amyloid polypeptide. *Biochim. Biophys. Acta* **1768:** 2002–2009.

Jones, T.A., Zou, J.Y., Cowan, S.W., and Kjeldgaard, M. 1991. Improved methods for building protein models in electron density maps and the location of errors in these models. *Acta Crystallogr. A* **47:** 110–119.

Kajava, A.V., Aebi, U., and Steven, A.C. 2005. The parallel superpleated β-structure as a model for amyloid fibrils of human amylin. **348:** 247–252.

Kapurniotu, A. 2001. Amyloidogenicity and cytotoxicity of islet amyloid polypeptide. *Biopolymers* **60:** 438–459.

Kodali, R. and Wetzel, R. 2007. Polymorphism in the intermediates and products of amyloid assembly. *Curr. Opin. Struct. Biol.* **17:** 48–57.

Konarkowska, B., Aitken, J.F., Kistler, J., Zhang, S., and Cooper, G.J.S. 2006. The aggregation potential of human amylin determines its cytotoxicity towards islet β-cells. *FEBS J.* **273:** 3614–3624.

Koo, B.W. and Miranker, A.D. 2005. Contribution of the intrinsic disulfide to the assembly mechanism of islet amyloid. *Protein Sci.* **14:** 231–239.

Larson, J.L. and Miranker, A.D. 2004. The mechanism of insulin action on islet amyloid polypeptide fiber formation. *J. Mol. Biol.* **335:** 221–231.

Lawrence, M.C. and Colman, P.M. 1993. Shape complementarity at protein/protein interfaces. *J. Mol. Biol.* **234:** 946–950.

Luca, S., Yau, W.M., Leapman, R., and Tycko, R. 2007. Peptide conformation and supramolecular organization in amylin fibrils: Constraints from solid-state NMR. *Biochemistry* **46:** 13505–13522.

Moriarty, D.F. and Raleigh, D.P. 1999. Effects of sequential proline substitutions on amyloid formation by human amylin20-29. *Biochemistry* **38:** 1811–1818.

Nelson, R., Sawaya, M.R., Balbirnie, M., Madsen, A.O., Riekel, C., Grothe, R., and Eisenberg, D. 2005. Structure of the cross-β spine of amyloid-like fibrils. *Nature* **435:** 773–778.

Nishi, M., Chan, S.J., Nagamatsu, S., Bell, G.I., and Steiner, D.F. 1989. Conservation of the sequence of islet amyloid polypeptide in five mammals is consistent with its putative role as an islet hormone. *Proc. Natl. Acad. Sci.* **86:** 5738–5742.

Padrick, S.B. and Miranker, A.D. 2001. Islet amyloid polypeptide: Identification of long-range contacts and local order on the fibrillogenesis pathway. *J. Mol. Biol.* **308:** 783–794.

Ritzel, R.A., Meier, J.J., Lin, C.-Y., Veldhuis, J.D., and Butler, P.C. 2007. Human islet amyloid polypeptide oligomers disrupt cell coupling, induce apoptosis, and impair insulin secretion in isolated human islets. *Diabetes* **56:** 65–71.

Saltiel, A.R. 2001. New perspectives into the molecular pathogenesis and treatment of type 2 diabetes. *Cell* **104:** 517–529.

Sawaya, M.R., Sambashivan, S., Nelson, R., Ivanova, M.I., Sievers, S.A., Apostol, M.I., Thompson, M.J., Balbirnie, M., Wiltzius, J.J.W., McFarlane, H.T., et al. 2007. Atomic structures of amyloid cross-β spines reveal varied steric zippers. *Nature* **447:** 453–457.

Schmitz, O., Brock, B., and Rungby, J. 2004. Amylin agonists: A novel approach in the treatment of diabetes. *Diabetes* **53:** S233–S238.

Sumner Makin, O. and Serpell, L.C. 2004. Structural characterisation of islet amyloid polypeptide fibrils. *J. Mol. Biol.* **335:** 1279–1288.

Tenidis, K., Waldner, M., Bernhagen, J., Fischle, W., Bergmann, M., Weber, M., Merkle, M.-L., Voelter, W., Brunner, H., and Kapurniotu, A. 2000. Identification of a penta- and hexapeptide of islet amyloid polypeptide (IAPP) with amyloidogenic and cytotoxic properties. *J. Mol. Biol.* **295:** 1055–1071.

Thompson, M.J., Sievers, S.A., Karanicolas, J., Ivanova, M.I., Baker, D., and Eisenberg, D. 2006. The 3D profile method for identifying fibril-forming segments of proteins. *Proc. Natl. Acad. Sci.* **103:** 4074–4078.

Tracz, S.M., Abedini, A., Driscoll, M., and Raleigh, D.P. 2004. Role of aromatic interactions in amyloid formation by peptides derived from human amylin. *Biochemistry* **43:** 15901–15908.

Tycko, R. 2004. Progress towards a molecular-level structural understanding of amyloid fibrils. *Curr. Opin. Struct. Biol.* **14:** 96–103.

Westermark, P., Wernstedt, C., Wilander, E., Hayden, D.W., O'Brien, T.D., and Johnson, K.H. 1987. Amyloid fibrils in human insulinoma and islets of Langerhans of the diabetic cat are derived from a neuropeptide-like protein also present in normal islet cells. *Proc. Natl. Acad. Sci.* **84:** 3881–3885.

Westermark, P., Engstrom, U., Johnson, K.H., Westermark, G.T., and Betsholtz, C. 1990. Islet amyloid polypeptide: Pinpointing amino acid residues linked to amyloid fibril formation. *Proc. Natl. Acad. Sci.* **87:** 5036–5040.

Yan, L.-M., Tatarek-Nossol, M., Velkova, A., Kazantzis, A., and Kapurniotu, A. 2006. Design of a mimic of nonamyloidogenic and bioactive human islet amyloid polypeptide (IAPP) as nanomolar affinity inhibitor of IAPP cytotoxic fibrillogenesis. *Proc. Natl. Acad. Sci.* **103:** 2046–2051.